

Spin coating of non-Newtonian fluids with a moving front

J. P. F. Charpin,^{1,2} M. Lombe,³ and T. G. Myers^{2,*}

¹*MACSI, Department of Maths and Statistics, University of Limerick, Limerick, Ireland*

²*Department of Maths and Applied Maths, University of Cape Town, Rondebosch 7701, South Africa*

³*Department of Maths and Statistics, University of Zambia, P.O. Box 32379, Lusaka, Zambia*

(Received 21 September 2006; revised manuscript received 7 March 2007; published 24 July 2007)

We investigate axisymmetric spin coating of power law and Ellis fluids. The flow is driven by centrifugal force, gravity and surface tension. For power law and Ellis models a single equation for the fluid film height is obtained. For a Newtonian fluid the flux only involves linear derivative terms which allows the flux to be easily split for a numerical scheme. For power law and Ellis models the derivatives appear as nonlinear terms. To overcome this we develop an alternative numerical scheme to solve for the film height. Neglecting surface tension and gravity the power law model shows a central spike which is reduced by the introduction of surface tension and gravity. In certain cases the shear thinning power law model predicts slower spreading than the Newtonian model. The Ellis fluid shows no central spike, even for zero surface tension and the film always spreads further than the Newtonian fluid.

DOI: [10.1103/PhysRevE.76.016312](https://doi.org/10.1103/PhysRevE.76.016312)

PACS number(s): 47.50.-d, 47.11.-j, 68.15.+e

I. INTRODUCTION

Spin coating is a widely used procedure in industrial applications. It is used in the production of certain types of semiconductors, magnetic disk coating, CDs, DVDs, antireflection coatings, and television tube phosphor coatings [1–5]. Consequently, there has been a significant amount of research directed at understanding and so controlling the process.

Since the coating layer is thin, it is sensible to model the spin coating process using lubrication theory and many researchers have followed this route. The original lubrication model was developed by Emslie, Bonner, and Peck [6]. Their model involved a balance between the centrifugal force driving fluid outwards and viscous resistance opposing this motion. The fluid was assumed to be Newtonian. Subsequently, their model has been enhanced by numerous researchers to include effects such as surface shear, evaporation, Coriolis force, surface roughness, and surface tension, see Refs. [2,7–10], for example. Perhaps the most advanced model to date is presented in Ref. [11], where the flow is driven by surface tension, gravity, centrifugal and Coriolis forces, and disjoining pressure. Their primary goal is to predict finger formation, and their numerical results show good agreement with published experimental work.

However, in industrial applications the fluid of interest is seldom Newtonian. Typical coating fluids exhibit Newtonian behavior at very high and very low shear rates and are shear thinning at moderate shear rates. Most polymeric fluids fit this description, as do certain suspensions [12–14]. These fluids are often referred to as having structural viscosity since the change in viscosity may be associated with a breakdown of the structure which subsequently recovers upon removal of the stress. Mud, blood, ice, and fluidised beds have

also been modelled as having some form of structural viscosity [15–18].

The most popular non-Newtonian fluid model is the power law model

$$\eta = K|\dot{\gamma}|^{n-1}, \quad (1)$$

where η is the dynamic viscosity, $\dot{\gamma}$ is the shear rate, n is the power law index, and K is known as the consistency. This model is simple to manipulate and can, in many cases, lead to analytical solutions. It has been used with great success in modeling industrial flows. However, it should be applied with care. It cannot capture the high and low shear Newtonian regions. This is not a great concern for the high shear rate plateau which is associated with a breakdown of the fluid structure and will seldom be reached in spin coating applications. However, the low shear rate region does cause problems. For shear thinning fluids $n < 1$, if the shear rate is zero then the model predicts infinite viscosity. This is particularly dangerous when modeling thin film flows, where the region of unrealistically high viscosity can form a significant part of the flow. In Ref. [19], it is shown that previous models using the power law relation and lubrication theory can lead to wildly inaccurate flow predictions. Other difficulties with the power law model are discussed in Ref. [20].

A more realistic model is the Ellis model, see Refs. [13,19,20], for example. This expresses the viscosity as a function of the shear stress

$$\eta = \eta_0 \left(1 + \left| \frac{\tau}{\tau_{1/2}} \right|^{\alpha-1} \right)^{-1}, \quad (2)$$

where η_0 is the viscosity at zero shear, τ is the shear stress, and $\tau_{1/2}$ is the shear stress where the viscosity is half of its initial value. The exponent α plays a role similar to $1/n$ in the power law model $\alpha > 1$ and $\alpha < 1$ corresponds to shear thinning and shear thickening fluids, respectively. The Ellis model does capture the low shear rate plateau and so does not suffer from the same malady as the power law model. For certain fluids the Carreau model has been suggested as

*Present address: Division of Applied Mathematics, KAIST 373-1 Guseong-dong, Yuseong-gu, Daejeon 305-701, Korea. E-mail: myers@maths.uct.ac.za

providing an even better description of the viscosity, particularly in the vicinity of the transition from Newtonian to power law behavior, see Refs. [12,13]

$$\eta \approx \eta_0(1 + \lambda_c^2 \dot{\gamma}^2)^{(n-1)/2}. \quad (3)$$

However, Myers [19] has shown that for thin film flows, where the shear rate seldom reaches extremely high values, Ellis and Carreau models can lead to equivalent results with an appropriate choice of parameters. The main reason for choosing Ellis over Carreau is that Ellis permits greater analytical progress. In particular, when using the thin film approximation, a standard mass balance for the film height may be written down, with an analytical expression for the flux. With the Carreau model numerical integration is required to determine the velocity and a further numerical integration then gives the flux.

In the following work we will detail an investigation into the axisymmetric spin coating of non-Newtonian fluids. Results for power law, Ellis, and Newtonian fluids will be presented. The model is unique in that the flow is driven by centrifugal force, gravity and surface tension. Previous work on spin coating of non-Newtonian fluids has neglected surface tension. We also develop an alternative numerical scheme in order to deal with the nonlinearity inherent to the governing equation.

The flow of a power law fluid, driven by centrifugal force, was investigated by Acrivos *et al.* [21]. Their results indicated that an initially uniform film would lose its uniformity. In fact the results showed that fluid near the center remained stationary and so formed a spike (contrary to experimental evidence). This is an obvious consequence of the viscosity model. At $r=0$ symmetry requires the shear rate to be zero, consequently the viscosity is infinite and the fluid is immobile. Close to $r=0$ the viscosity will remain high, resulting in a slow moving central region. As the exponent n decreases the area of the slow moving region increases resulting in a more pronounced spike. Subsequently, Jenekhe and Schuldt [22,23] demonstrated that the central spike was a consequence of applying the power law model at low shear rates. They dealt with fluids of infinite extent and three initial profiles and solved the problem numerically, using a Carreau fluid model. Their results showed that a film with initially uniform height evolved with an approximately uniform height, while non-uniform films rapidly became approximately uniform. They concluded that power law fluids were unsuitable for modeling axisymmetric free surface flows. Recently, Myers [19] reached a similar conclusion for certain coating and pipe flows. Lawrence and Zhou [24] investigate power law, Ellis and Carreau-Yasuda models for centrifugally driven films. They conclude that the film should be flat near the center and slope away from there.

We commence our investigation by deriving the governing equations for spin coating of power law and Ellis fluids. The standard Newtonian model can be retrieved from either model by an appropriate choice of parameters. The numerical solution is then described. A scheme for the Newtonian model will be considered first and a simple extension to non-Newtonian fluids is then presented. Finally, numerical results

will be presented for both Newtonian and non-Newtonian models in Sec.III.

II. GOVERNING EQUATIONS

We begin our analysis with the standard lubrication approximation to the Navier-Stokes equations. The model requires the following assumptions The plane is smooth, has an infinite radius (edge effects may be neglected) and rotates at a constant angular velocity Ω . The flow is such that lubrication theory may be applied, this means ϵ^2 , $\epsilon^2 \text{Re} \ll 1$, where ϵ is the aspect ratio of the flow and Re the Reynolds number. There is no slip between the fluid and the solid. The shear stress due to the induced air flow is negligible. The flow is axisymmetric.

A. Mass balance derivation

Using the standard scaling for lubrication theory, the governing equations may be written

$$0 = \frac{1}{r} \frac{\partial(ru)}{\partial r} + \frac{\partial w}{\partial z}, \quad (4)$$

$$0 = -\frac{\partial p}{\partial r} + \frac{2\rho\Omega H^2 LV}{\bar{\eta}U}v + \frac{\rho\Omega^2 H^2 L}{\bar{\eta}U}r + \frac{\partial}{\partial z} \left(\eta \frac{\partial u}{\partial z} \right) + O(\epsilon^2, \epsilon^2 \text{Re}), \quad (5)$$

$$0 = -\frac{2\epsilon^2 \rho \Omega L^2 U}{\bar{\eta}V}u + \frac{\partial}{\partial z} \left(\eta \frac{\partial v}{\partial z} \right) + O(\epsilon^2, \epsilon^2 \text{Re}), \quad (6)$$

$$0 = -\frac{\partial p}{\partial z} - \frac{\rho g H^3}{\bar{\eta}LU} + O(\epsilon^2, \epsilon^2 \text{Re}). \quad (7)$$

The various symbols are as follows: p is the fluid pressure; u, v are the radial and azimuthal velocities; L, H are the length scales in the radial and vertical directions; $\epsilon = H/L \ll 1$; Ω is the rotation speed; ρ the fluid density; and $\bar{\eta}$ the viscosity scale. The second term on the right-hand side of Eq. (5) represents the Coriolis force, the third is the centrifugal term. In Eq. (6) the first term on the right hand side represents the Coriolis force. As shown in Refs. [8,10], the centrifugal force drives the flow in the radial direction and Coriolis drives the flow in the azimuthal direction. Equations (5) and (6) determine the velocity scales in the r and θ directions $U = \rho\Omega^2 H^2 L / \bar{\eta}$ and $V = 2\epsilon^2 \rho \Omega L^2 U / \bar{\eta}$.

If the velocity scale V is substituted into Eq. (5) we find that the term involving v is of $O(\epsilon^2 \text{Re})$ and therefore negligible at leading order. This point is the crux of current debate on the effect of the Coriolis force. For axisymmetric flow the film height is determined by integrating the leading order terms in Eq. (5) to determine the radial flux. This is then combined with the continuity equation to give the standard mass balance that determines the film height. So, for axisymmetric flow, the Coriolis force does not affect the film height at leading order. It does, however, affect the azimuthal velocity since the choice of V makes the nondimensional form of Eq. (6)

$$\frac{\partial}{\partial z} \left(\eta \frac{\partial v}{\partial z} \right) - u = 0. \quad (8)$$

At leading order Coriolis is then the sole driving force for azimuthal flow. Schwartz and Roy [11] focus on nonaxisymmetric flow and finger formation. They state that the Coriolis correction appears at leading order, in agreement with Momoniat and Mason [25], and that researchers who find it at lower order, such as Ref. [10], do so due to an *ab initio* assumption that the flow is axisymmetric. However, the actual statement made in Ref. [10] is that for axisymmetric flow “the Coriolis term in the radial velocity equation is negligible.” The analysis in Ref. [10], in fact, shows that Coriolis enters the azimuthal equation at leading order. Since it is the radial equation that determines the film height it is correct to neglect the Coriolis force at leading order in axisymmetric flow. This has subsequently been clarified in Ref. [8].

Now, since we are working with axisymmetric flow we can neglect Eq. (6), as well as the term involving v in Eq. (5) and are left with the following nondimensional system:

$$0 = \frac{1}{r} \frac{\partial(ru)}{\partial r} + \frac{\partial w}{\partial z}, \quad (9)$$

$$0 = -\frac{\partial p}{\partial r} + r + \frac{\partial}{\partial z} \left(\eta \frac{\partial u}{\partial z} \right), \quad (10)$$

$$0 = -\frac{\partial p}{\partial z} - B, \quad (11)$$

where $B = \rho g H^3 / (\bar{\eta} L U)$ is the Bond number.

Appropriate boundary conditions for Eqs. (9)–(11) are

$$u = w = 0 \Big|_{z=0}, \quad \frac{\partial u}{\partial z} \Big|_{z=h} = 0, \quad (12)$$

$$w = \frac{\partial h}{\partial t} + u \frac{\partial h}{\partial r} \Big|_{z=h}, \quad p - p_0 = -C \nabla^2 h \Big|_{z=h}, \quad (13)$$

which represent the standard no-slip, zero shear, kinematic condition, and normal stress boundary conditions, respectively. The constant p_0 represents the ambient pressure and C is the inverse capillary number $C = \epsilon^3 \sigma / (\bar{\eta} U)$, where σ is the surface tension.

The leading order pressure within the fluid may be obtained by integrating Eq. (11):

$$p = p_0 - B(z - h) - C \nabla^2 h. \quad (14)$$

Integrating the continuity equation (9) subject to the no-slip condition determines w , which in turn may be used with the kinematic condition to give the usual mass balance

$$\frac{\partial h}{\partial t} + \frac{1}{r} \frac{\partial(rQ)}{\partial r} = 0, \quad (15)$$

where

$$Q = \int_0^h u dz.$$

To determine the flux Q we must obtain an expression for u . This comes from integrating Eq. (10). In order to do this we must specify the viscosity η , so we now detail the two models to be used, namely the power law and Ellis models.

B. Power law model

In the power law model, the dynamic viscosity is described by Eq. (1). The appropriate nondimensional shear rate to use in this equation is

$$\dot{\gamma} = \sqrt{\epsilon^2 \left(\frac{\partial u}{\partial r} \right)^2 + \left(\frac{\partial u}{\partial z} \right)^2} \approx \left| \frac{\partial u}{\partial z} \right| = \lambda \frac{\partial u}{\partial z}.$$

This scaling does lead to problems near the free surface, where $u_z = O(\epsilon)$, in which case both terms balance and $\dot{\gamma} = O(\epsilon)$. One solution would be to re-scale the whole problem in this boundary layer and match solutions. This approach has been adopted in Ref. [26] when explaining a classical problem associated with applying thin film theory to Bingham fluids. We choose to neglect this issue since this boundary layer has a negligible effect on the fluid velocity and film height. The velocity is primarily determined by the flow in the high shear region near the substrate, see Ref. [19]. We introduce the parameter $\lambda = \pm 1$ to represent the sign of the velocity gradient. In this way we avoid algebraic difficulties associated with the modulus sign. A straightforward integration of Eq. (9) proves that λ is constant throughout the depth of the flow and may only vary with the radius r . In general, we expect $\lambda = 1$, since the flow is radially outwards and the velocity increases from zero at $z=0$ to a maximum at $z=h$. In the case of zero gravity and surface tension, $B=0$ and $C=0$, this is true everywhere and we can set $\lambda=1$. However, with $B \neq 0$ or $C \neq 0$ there are regions near the contact line with $u_z < 0$ rendering the use of the modulus sign or λ necessary. The viscosity is defined as

$$\bar{\eta} \eta = K \left(\frac{U}{H} \right)^{n-1} \left(\lambda \frac{\partial u}{\partial z} \right)^{n-1}. \quad (16)$$

For the power law model, the viscosity scale $\bar{\eta}$ is then

$$\bar{\eta} = K \left(\frac{U}{H} \right)^{n-1}.$$

The velocity scale $U = \rho \Omega^2 H^2 L / \bar{\eta}$ may be explicitly defined as

$$U = \left(\frac{\rho \Omega^2 H^{n+1} L}{K} \right)^{1/n}.$$

Integrating Eq. (10) and applying Eq. (12) leads to

$$u = \frac{\lambda n}{n+1} \left\{ \lambda \left(C \frac{\partial}{\partial r} \left[\frac{1}{r} \frac{\partial}{\partial r} \left(r \frac{\partial h}{\partial r} \right) \right] - B \frac{\partial h}{\partial r} + r \right) \right\}^{1/n} \times [h^{(n+1)/n} - (h-z)^{(n+1)/n}].$$

The flux Q is then given by

$$Q = \frac{\lambda n}{2n+1} h^{2+1/n} \left(\lambda \left\{ C \frac{\partial}{\partial r} \left[\frac{1}{r} \frac{\partial}{\partial r} \left(r \frac{\partial h}{\partial r} \right) \right] - B \frac{\partial h}{\partial r} + r \right\} \right)^{1/n}. \quad (17)$$

Substituting Eq. (17) into Eq. (15) gives the single equation which determines the film height for the axisymmetric flow of a power law fluid on a rotating disk. The standard Newtonian model is retrieved by setting $\lambda=n=1$.

C. Ellis model

Now the viscosity is described by Eq. (2). The shear stress in Eq. (2) may be expressed in terms of the viscosity and shear rate

$$\tau = \eta \dot{\gamma} \approx \eta \lambda \frac{\partial u}{\partial z}.$$

The nondimensional viscosity is

$$\eta = \frac{\eta_0}{\bar{\eta}} \left[1 + \beta^{-1} \left(\lambda \eta \frac{\partial u}{\partial z} \right)^{\alpha-1} \right]^{-1},$$

where $\beta = (H\tau_{1/2}/\bar{\eta}U)^{\alpha-1}$ and $\lambda = \pm 1$ is the sign of the velocity gradient, and here again this value may only vary with the radius r . This gives us two choices for velocity scale. The Newtonian scale simply has $\bar{\eta} = \eta_0$, however, if we expect non-Newtonian effects to dominate then the best choice is $\bar{\eta} = \eta_0 \beta$ and since β involves $\bar{\eta}$ this reduces to

$$\bar{\eta} = \eta_0^{1/\alpha} \left(\frac{H\tau_{1/2}}{U} \right)^{(\alpha-1)/\alpha}.$$

The velocity scale is then

$$U = \frac{(\rho\Omega^2 L)^\alpha H^{\alpha+1}}{\eta_0^{\alpha-1} \tau_{1/2}^{\alpha-1}}.$$

Integrating Eq. (10) and applying Eq. (12) leads to an expression for the radial velocity. Integrating again gives the flux Q :

$$Q = \frac{\beta h^3}{3} \left\{ C \frac{\partial}{\partial r} \left[\frac{1}{r} \frac{\partial}{\partial r} \left(r \frac{\partial h}{\partial r} \right) \right] - B \frac{\partial h}{\partial r} + r \right\} + \frac{\lambda h^{\alpha+2}}{\alpha+2} \left(\lambda \left\{ C \frac{\partial}{\partial r} \left[\frac{1}{r} \frac{\partial}{\partial r} \left(r \frac{\partial h}{\partial r} \right) \right] - B \frac{\partial h}{\partial r} + r \right\} \right)^\alpha. \quad (18)$$

Combining this expression with the mass balance (15) gives the governing equation to determine the film height for an Ellis fluid. We retrieve the standard Newtonian model by letting $\beta \rightarrow \infty$, so that the Newtonian terms dominate the velocity and flux expressions. We would also have to alter the velocity scale U , which tends to zero as $\beta \rightarrow \infty$, to reflect the fact that Newtonian rather than non-Newtonian flow dominates. Little analytical progress is possible for either the Ellis or power law models, so we now describe the numerical solution method.

III. NUMERICAL RESULTS

The method to solve the governing equation (15) is standard for a Newtonian fluid. In this section we will briefly

describe the modification for non-Newtonian fluids before presenting the numerical results.

The Newtonian problem has a well known difficulty at the moving contact line, where the shear stress has a non-integrable stress singularity. This problem does not occur with shear thinning fluids where the viscosity $\eta \rightarrow 0$ as the shear stress $\tau \rightarrow \infty$, see Refs. [11,19,27,28]. However, in the following we will still use a standard technique for removing the singularity in Newtonian flow, by incorporating a precursor film. This allows us to compare Newtonian and non-Newtonian solutions and also avoids any potential difficulty as the model parameters are reduced towards the Newtonian values. Another difficulty is that over most of the domain, the dominant term in the flux is the centrifugal force. If this is used as the sole driving force then the solution will develop a shock at the leading edge. To prevent this we must therefore include the surface tension and gravity terms. The fourth-order surface tension term in particular significantly complicates any numerical scheme, yet it is clearly necessary if we wish to avoid the shock. A difficulty specific to the non-Newtonian problem is caused by the powers $1/n$ and α in the power law and Ellis models. The form of the flux, with these nonlinear terms, prevents us from splitting the flux in a standard manner and therefore requires an alternative type of numerical scheme.

For the Newtonian problem we split the flux into two components: the first, Q_c , contains only the centrifugal term, the second, Q_d , contains the diffusive terms, namely surface tension and gravity. To prevent a shock the flux Q_c is discretized with an upwind scheme while a centered scheme is used for Q_d . The fluid height may then be calculated with a number of standard methods. However, to reduce computing time we employ the semi-implicit algorithm suggested by Ref. [9]. Using this method the derivatives of h are expressed implicitly while h^3 is expressed explicitly. When dealing with non-Newtonian fluids we modify the semi-implicit method by first writing the governing equation in the form

$$\frac{\partial h}{\partial t} + \frac{1}{r} \frac{\partial (r\theta Q^N)}{\partial r} = 0, \quad (19)$$

where Q^N is the Newtonian flux and $\theta = Q^{NN}/Q^N$ is the ratio of non-Newtonian to Newtonian fluxes. For a power law fluid

$$\theta = \frac{Q^{NN}}{Q^N},$$

$$= \frac{3n}{2n+1} h^{(1-n)/n} \left| -\frac{\partial p}{\partial r} + \chi r \right|^{(1-n)/n},$$

and for Ellis fluids

$$\theta = \beta + \frac{3}{\alpha+2} h^{\alpha-1} \left| -\frac{\partial p}{\partial r} + \chi r \right|^{\alpha-1}.$$

Replacing the fluxes Q by the product θQ in the method used for Newtonian fluids provides the numerical algorithm for Eq. (19). All terms in θ are evaluated explicitly. The ratio also includes the correction factor χ , this guarantees that the numerical scheme reduces to an upwind scheme when the

Bond and inverse capillary number, B and C , become very small:

$$\chi^{\text{power law}} = \left(\frac{Q_c^{\text{up}}}{Q_c^{\text{cen}}} \right)^{2n+1}, \quad \chi^{\text{Ellis}} = \left(\frac{Q_c^{\text{up}}}{Q_c^{\text{cen}}} \right)^{1+2/\alpha},$$

where Q_c^{up} and Q_c^{cen} denote the upwind and central discretisation of the centrifugal flux Q_c respectively.

Throughout this section the results will be computed with the initial height

$$h(r) = 1 - r^2 \quad \text{if } 0 \leq r \leq \sqrt{1 - h_p},$$

$$h(r) = h_p, \quad \text{otherwise,}$$

with the precursor film $h_p = 0.001$.

The velocity and time scale U and T and the nondimensional parameters B and C are functions of the fluid density ρ , the typical value of the dynamic viscosity $\bar{\eta}$, the surface tension σ , and the viscosity model. To evaluate the effects of the different viscosity models, for all the fluids considered, typical values for water are used:

$$\rho = 1000 \text{ kg m}^{-3}, \quad \sigma = 0.0728 \text{ kg s}^{-2}, \quad K = \eta_0 = 0.001,$$

and the unit of this last parameter varies with the model. With these values similar for all fluids, the differences in the profiles are due solely to the viscosity model.

All simulations are carried out with $\Delta r = 0.001$ and $\Delta t = 0.001$ except when $n = 0.5$ and $\alpha = 2$ where the space step is $\Delta r = 0.002$. Unless specified otherwise the rotation rate $\Omega = 2\pi$ rad/s and $B = 0.017$, $C = 8.9 \times 10^{-6}$.

A. Newtonian fluids

As an initial test of the numerical scheme we compared numerical results for the case $B = C = 0$ with the known analytical solution to Eq. (15) with $Q = rh^3/3$,

$$r = r_0 \left(1 + \frac{4}{3} h_0^2 t \right)^{3/4}, \quad h = h_0 \left(1 + \frac{4}{3} h_0^2 t \right)^{-1/2}, \quad (20)$$

where (r_0, h_0) denotes the position of the particle at (r, h) at time $t = 0$. For small times the results were indistinguishable. For larger times a shock forms and the analytical solution becomes multivalued. However, over the central region the film heights are still indistinguishable.

In Fig. 1 we show numerical results with $B = 0.017$ and $C = 8.9 \times 10^{-6}$. The small values of B and C mean that this is still a centrifugally dominated flow. The only real difference between this and the results when $B = C = 0$ is the capillary ridge that forms before the moving front. The size of the ridge varies with the inverse capillary number C , which varies with the speed of rotation Ω , $C \sim \Omega^{-2}$. This can be more clearly seen in Fig. 2.

When $C = 0$ there can be no capillary ridge. This solution must coincide with the large Ω solution. As C increases or Ω decreases, so does the ridge height and width. The spreading rate also decreases slightly. Of course, this is what we would expect, as Ω decreases the centrifugal force decreases and so the fluid is not thrown outwards at such a high rate. Increasing surface tension also means that the fluid is held together

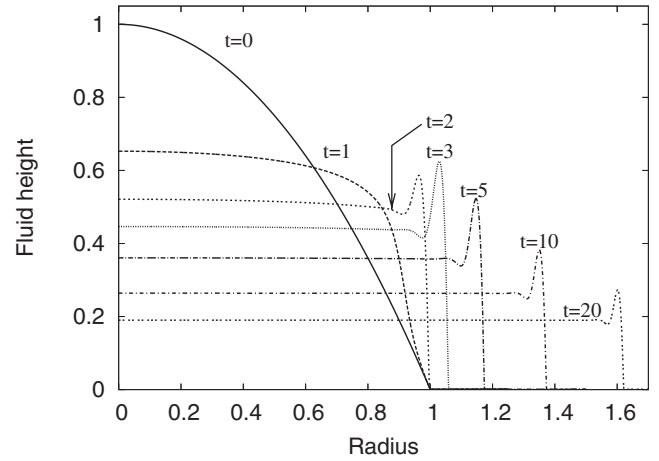


FIG. 1. Evolution of a Newtonian fluid with $B = 0.017$, $C = 8.9 \times 10^{-6}$.

more strongly. The exact values for B and C for the different rotation rates shown in Fig. 2 are $(\Omega, B, C) = (2\pi, 0.017, 8.9 \times 10^{-6})$, $(4\pi, 4.3 \times 10^{-3}, 2.2 \times 10^{-6})$, $(10\pi, 6.9 \times 10^{-4}, 3.6 \times 10^{-7})$, $(20\pi, 1.7 \times 10^{-4}, 8.9 \times 10^{-9})$. These results are typical for thin film flows and well known, so we will now move on to the non-Newtonian models, starting with the power law fluid.

B. Power law fluids

As with the Newtonian model we tested our numerical scheme against an analytical one when $B = C = 0$. The analytical curves are given by

$$r = r_0 \left(1 + \frac{3n+1}{2n+1} h_0^{1+1/n} r_0^{(n-1)/n} t \right)^{(2n+1)/(3n+1)}, \quad (21)$$

$$h = h_0 \left(1 + \frac{3n+1}{2n+1} h_0^{1+1/n} r_0^{(n-1)/n} t \right)^{-(n+1)/(3n+1)}, \quad (22)$$

where (r_0, h_0) denotes the position of the particle at (r, h) at time $t = 0$. The term $r_0^{(1-n)/n}$ in Eqs. (21) and (22) shows that the point originally at $r_0 = 0$, $h_0 = 1$ remains in that position

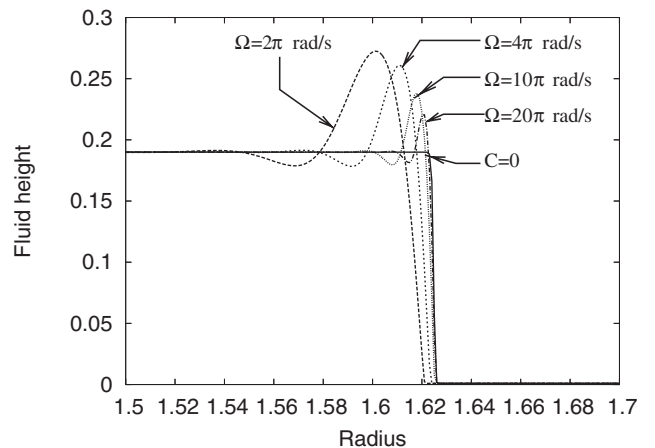


FIG. 2. Front wave with various rotation velocities at $t = 20$.

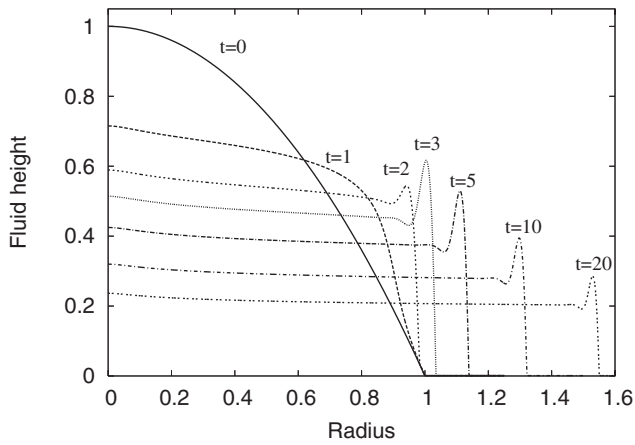


FIG. 3. Evolution of a power law fluid with $n=0.9$, $B=0.017$, $C=8.9 \times 10^{-6}$.

for all time. Hence at the center, the analytical curve has $h = 1$ for all time. This is an obvious consequence of the viscosity model. At $r=0$ symmetry requires the shear rate to be zero, the viscosity is therefore infinite and no motion is possible. This effect is also observed in the numerical results. Again the numerical and analytical results are virtually identical, except for near the moving contact line where the analytical solution is multivalued.

Figure 3 shows the evolution of the fluid profile for $0 \leq t \leq 20$. The differences between this result and the case $B=C=0$ only occur near the rotating axis, $r=0$ and at the contact line. Around $r=0$, surface tension and gravity act to push the fluid down, the surface tension force in particular is proportional to curvature and so the peak at the center is reduced. As with Newtonian fluids, near the contact line a front wave appears and prevents the shock from developing in a nonphysical manner. The wave appears around $t \approx 1.5$ and grows to reach its maximum when the fluid starts spreading, shortly before $t=3$. From this moment, the height of the fluid bulk decreases progressively. The curvature of the profile near the front becomes lower and the amplitude of the wave diminishes.

The effects of gravity and surface tension at the two extremities vary significantly with the rotation velocity, as

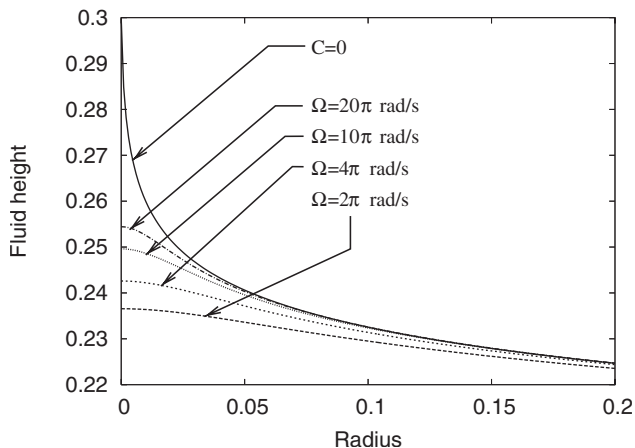


FIG. 4. Center with various rotation velocities $n=0.9$, $t=20$.

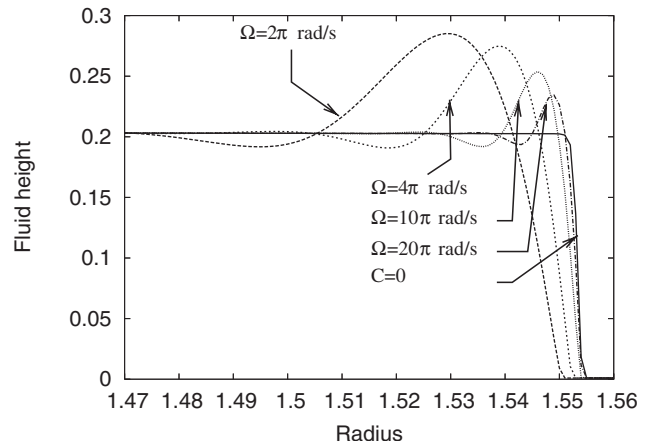


FIG. 5. Front wave with various rotation velocities $n=0.9$, $t=20$.

shown in Figs. 4 and 5. When the rotation velocity Ω increases, the Bond and inverse capillary numbers decrease and the smoothing effect at the center of the flow also decreases. The values for B and C vary in the same way with Ω as detailed in the previous section. Although the curve remains flat at $r=0$, the gradient in the vicinity of $r=0$ becomes much higher and the peak at the center reappears.

Finally, the curves are compared in Fig. 6 for different values of the parameter n at the dimensional time $t=0.01$ s. We use a dimensional time since the time scale $T=L/U$ depends on n . The curves indicate that, in general, decreasing n leads to greater spreading. This is to be expected since $n < 1$ corresponds to a shear thinning fluid and as n decreases the shear thinning increases. When $n=1$ we see that the Newtonian fluid has hardly moved, with $n=0.5$ it has spread to $r \sim 2.8$. However, the weakly non-Newtonian fluid, $n=0.9$, remains very close to the Newtonian fluid and near the center it has a greater height. This highlights one flaw of the power law model. Despite the fact the fluid is shear thinning the flow is slower than the Newtonian fluid.

C. Ellis fluids

Ellis fluids are described by the flux expression (18) and are a mixture of Newtonian and power law models, with the

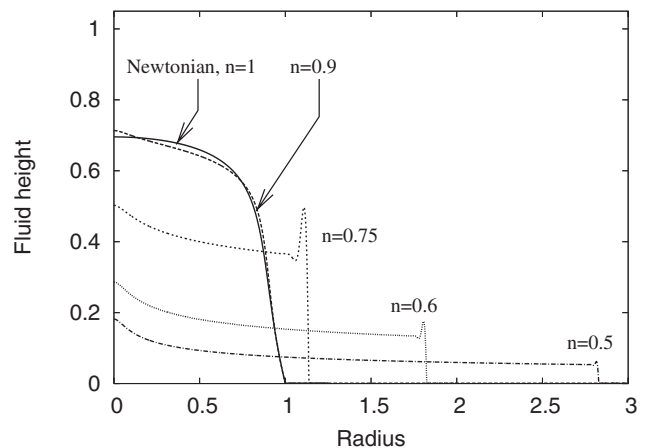


FIG. 6. Profiles for various power law indices.

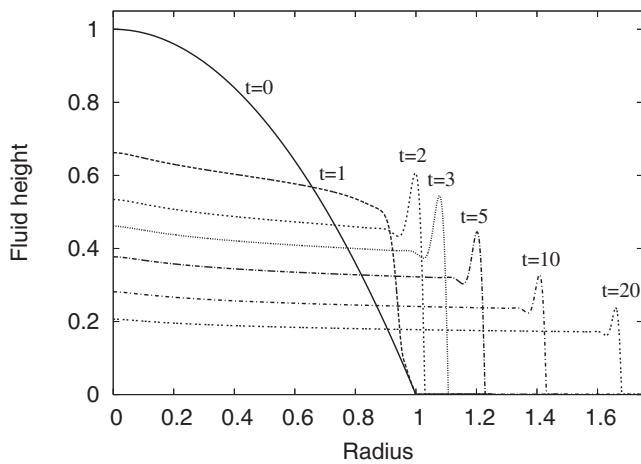


FIG. 7. Evolution of an Ellis fluid with $\alpha=4/3$, $\tau_{1/2}=5 \times 10^{-4}$.

power α corresponding to $1/n$. The balance between the models is determined by the coefficient β . For small values of β (when $\tau_{1/2}$ is small or Ω is large) the fluid will behave like a power law fluid, for large values (large $\tau_{1/2}$ or small Ω) Newtonian effects will dominate. Ellis profiles should therefore display characteristics observed in the two previous sections.

The evolution of an Ellis fluid between $0 \leq t \leq 20$ may be seen in Fig. 7. As anticipated, the fluid layer rapidly evolves during early times. The initial parabolic profile transforms into a nearly flat layer with a moving front. The fluid bulk is slightly inclined, less than the corresponding power law profile, and no peak appears near the center. This reflects the properties of an Ellis fluid. At the center, the power law component of the flux is very small and the Newtonian component dominates. The fluid may be viscous but the value of nondimensional viscosity η may not exceed 1 (in contrast to the infinite viscosity predicted by the power law model). The slope observed in the fluid bulk is a result of the power law component. When the radius increases, so does the shear rate, the fluid becomes less viscous and therefore tends to flow faster. Near the front, the usual front wave appears.

The fluid moves more easily when the parameter α is large. Figure 8 shows the extension of the fluid layer for the

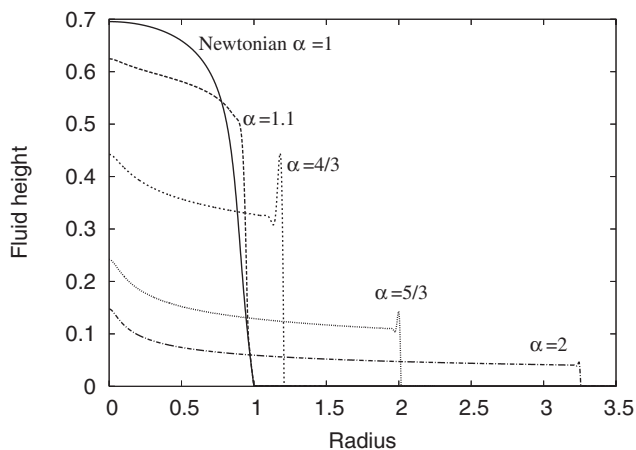


FIG. 8. Profiles for various Ellis indices, $\tau_{1/2}=5 \times 10^{-4}$.

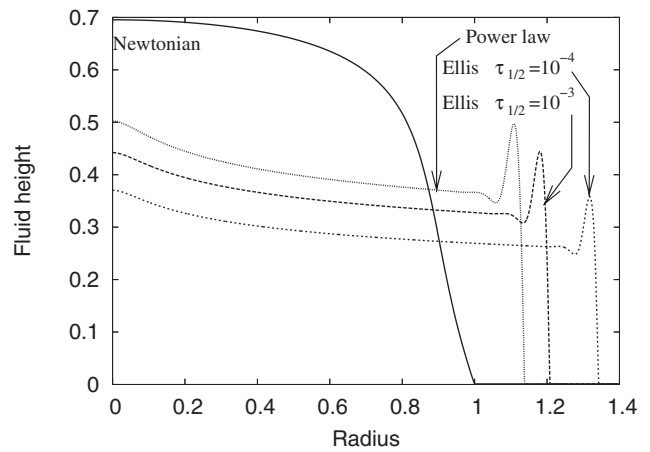


FIG. 9. Profiles for various models $n=0.75$, $\alpha=4/3$.

values of α corresponding to the values of n studied in Fig. 6 at the dimensional time $t=0.01$ s (recall $\alpha \sim 1/n$). The film height for $\alpha=2$ has spread furthest, to $r \approx 3.25$. The corresponding power law film, with $n=0.5$, only reached $r \approx 2.8$. Perhaps more significant is the motion of the weakly non-Newtonian fluid. In Fig. 6 we saw that when $n=0.9$ the central height exceeded the Newtonian height and in general the curves were similar. The corresponding Ellis model, with $\alpha = 1.1$, shows a maximum height around 12% below the Newtonian value. The profiles clearly show how the combination of Newtonian and power law models affects the flow. Near the center Newtonian behavior dominates, and so the fluid can move more easily than a power law fluid. Away from the center the power law behavior dominates, this results in a sloping bulk region that spreads rapidly. As the index α increases, the fluid becomes more shear thinning and the spreading rate increases.

Finally, in Figs. 9 and 10, film profiles are compared for the Newtonian, power law, and two Ellis models at the dimensional time $t=0.01$ s. Again we must use a dimensional time due to the different time scales for each model. The qualitative behavior is the same in all figures. The Newtonian fluid spreads the most slowly, the Ellis fluid with the lowest value of $\tau_{1/2}$ most rapidly. When the shear thinning is relatively weak, $n=0.75$, $\alpha=4/3$ the difference in spreading

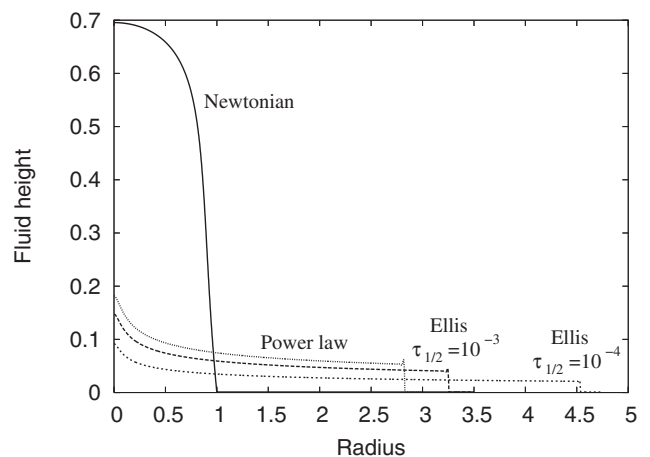


FIG. 10. Profiles for various models $n=0.5$, $\alpha=2$.

rates is relatively small. As n decreases and α increases the differences become more apparent. The final result, shown in Fig. 10, shows that the Newtonian fluid has not changed significantly from the original parabolic profile and remains at the original boundary at $r=1$, the Ellis fluid has a maximum height of 0.1, and has spread to $r \approx 4.5$.

IV. CONCLUSION

In this paper, a model was developed to describe axisymmetric spin coating including viscosity and centrifugal forces, gravity, and surface tension. The viscosity was described by Newtonian, power law, and Ellis models. The two non-Newtonian models were chosen since they allow the problem to be formulated in terms of a single equation for the film height. With a Newtonian fluid standard numerical techniques could be applied to determine the film height. In order to determine the film height for the non-Newtonian models an alternative numerical scheme had to be developed, using a semi-implicit scheme. We included a precursor film in each solution, even though it has been shown to be unnecessary for shear thinning fluids, since this provided a more sensible comparison between the Newtonian and non-Newtonian models and also allowed us to verify the non-Newtonian models by choosing parameter values corresponding to a Newtonian fluid.

The power law model has been the subject of previous studies of spin coating, although without the inclusion of surface tension. The results of Acrivos *et al.* [21] showed a central spike followed by a sloping region. Jenekhe *et al.* [22,23] demonstrated that the spike was an artifact of the power law model and that using a Carreau fluid model would remove this feature. However, the Carreau fluid model is not simple to use in free surface flows since the governing equation cannot be integrated analytically beyond the expression for the velocity gradient. The Ellis model can be integrated and leads to a mass balance for the film height. It is therefore significantly simpler to analyze the evolution of an Ellis fluid. Where comparison is possible, our results are in accord with those of Jenekhe. Namely, that the central spike is an artefact of the power law model when surface tension is neglected. This is an obvious consequence of the unrealistic infinite viscosity predicted by the power law model at the free surface and center line. However, since the surface tension stress is proportional to curvature, the inclusion of surface tension removes the spike. The spike becomes smoother and its height decreases as surface tension is increased. Hence, the spike may also be viewed as a consequence of neglecting surface tension. The infinite viscosity also means

that despite the fact the fluids modeled in this paper were shear thinning the flow of a power law fluid could be slower than Newtonian.

The Ellis model, which has a Newtonian plateau for low shear rates, does not suffer the infinite viscosity limitation. Consequently, the flow behavior was rather different to the power law fluid. In particular the Ellis fluid displayed more rapid spreading, even for cases where both Ellis and power law fluids displayed the same non-Newtonian behavior at high shear rates. As a Newtonian fluid spreads the film height becomes independent of r , except in the vicinity of the contact line. When surface tension is neglected the power law fluid has a sharp central peak. The Ellis fluid shows behavior characteristic of both power law and Newtonian films. A central peak remains, but it is lower and smoother. The film height also has a distinct slope up to the moving front, the degree of slope increases as the fluid becomes less Newtonian.

The numerical scheme developed for modeling the non-Newtonian flow was an extension of the standard Newtonian technique. For Newtonian fluids perhaps the most difficult feature is the fourth-order surface tension term appearing in the flux. However, in this case it is at least linear. With the non-Newtonian flows of this paper the fourth-order term appears in a nonlinear fashion. We dealt with this additional level of complexity by introducing a factor $\theta = Q^{NN}/Q^N$, the ratio of the non-Newtonian to Newtonian fluxes, where θ was calculated explicitly.

There are a number of obvious extensions to this work. We focussed primarily on shear-thinning fluids, but our scheme is also valid for shear thickening fluids. In this case the power law model leads to an unrealistic zero viscosity layer at the free surface and consequently spreads much more rapidly than the Ellis or Newtonian fluids. Many industrial fluids exhibit a yield stress and this would certainly be an interesting way forward. Our work is based on the assumption of axisymmetric flow. However, a driven front is unlikely to remain axisymmetric for long and will develop fingers. The Coriolis force would then have to be returned to the film height model.

ACKNOWLEDGMENTS

T.M. acknowledges the support of this work by the National Research Foundation of South Africa, under Grant No. 2053289 as well as the Korean Advanced Institute of Science and Technology. J.C. acknowledges the support of the Claude Leon Foundation. M.L. acknowledges the support of Third World Organisation for Women in Science (TWOWS).

-
- [1] R. G. Larson and T. G. Rehg, *Liquid Film Coating*, edited by S. F. Kistler and P. M. Schweizer (Chapman and Hall, London, 1997) Chap. Spin Coating, p. 709–734.
 [2] S. Middleman, *J. Appl. Phys.* **62**, 2530 (1987).
 [3] W. M. Moreau, *Semi-Conductor Lithography* (Plenum, New York 1988).

- [4] L. F. Thomson, C. G. Willson, and M. J. Bowden, *Introduction to Microlithography* (American Chemical Society, Washington, DC 1983).
 [5] http://www.disctronics.co.uk/technology/manuf/rep_metlac.htm. Last accessed 21/09/05.
 [6] A. G. Emslie, F. T. Bonner, and L. G. Peck, *J. Appl. Phys.* **29**,

- 858 (1958).
- [7] B. Reisfeld, S. G. Bankoff, and S. H. Davis, *J. Appl. Phys.* **70**, 5258 (1991).
- [8] T. G. Myers and M. Lombe, *Chem. Eng. Process.* **45**, 90 (2006).
- [9] J. A. Moriarty and L. W. Schwartz, *Phys. Fluids A* **3**, 733 (1991).
- [10] T. G. Myers and J. P. F. Charpin, *Int. J. Non-Linear Mech.* **36**, 629 (2001).
- [11] L. W. Schwartz and R. V. Roy, *Phys. Fluids* **16**, 569 (2004).
- [12] R. B. Bird, R. C. Armstrong, and O. Hassager, *Dynamics of Polymeric Fluids* (John Wiley & Sons, New York, 1977), Vol. 1.
- [13] *Encyclopedia of Fluid Mechanics*, edited by N. P. Cheremisinoff (Gulf Publishing, Texas, 1988), Vol. 7.
- [14] G. T. Helleloid, *Morehead Electron. J. Appl. Math.* **1**, 1 (2004).
- [15] Dredging Research Technical Notes No. DRP-2-04 (unpublished), <http://el.erdc.usace.army.mil/elpubs/pdf/drp2-04.pdf>
- [16] R. M. Johnston, P. R. Johnston, S. Corney, and D. Kilpatrick, *J. Biomech.* **37**, 709 (2004).
- [17] I. Machac, B. Siska, and Z. Lecjaks, *Chem. Pap.* **53**, 390 (1999).
- [18] A. V. Wilchinsky and D. L. Feltham, *Eur. J. Mech. B/Fluids* **23**, 681 (2004).
- [19] T. G. Myers, *Phys. Rev. E* **72**, 066302 (2005).
- [20] S. Matsuhisa and R. B. Bird, *AIChE J.* **11**, 588 (1965).
- [21] A. Acrivos, M. J. Shah, and E. E. Petersen, *J. Appl. Phys.* **31**, 963 (1960).
- [22] S. A. Jenekhe, *Polym. Eng. Sci.* **23**, 830 (1983).
- [23] S. A. Jenekhe and S. B. Schuldt, *Ind. Eng. Chem. Fundam.* **23**, 432 (1984).
- [24] C. J. Lawrence and W. Zhou, *J. Non-Newtonian Fluid Mech.* **39**, 137 (1991).
- [25] E. Momoniat and D. P. Mason, *Int. J. Non-Linear Mech.* **33**, 1069 (1998).
- [26] N. J. Balmforth and R. V. Craster, *J. Non-Newtonian Fluid Mech.* **84**, 65 (1999).
- [27] L. Ansini and L. Giacomelli, *Nonlinearity* **15**, 2147 (2002).
- [28] S. I. Betelu and M. A. Fontelos, *Math. Comput. Modell.* **40**, 729 (2004).